Automatic Picker Developments and Optimization: FilterPicker—a Robust, Broadband Picker for Real-Time Seismic Monitoring and Earthquake Early Warning

Anthony Lomax,[1] Claudio Satriano,[2, 3] and Maurizio Vassallo[3]

INTRODUCTION

Most earthquake location algorithms are based on ray-theory travel-times and thus require as input data the onset times of body-wave phases such as *P* and *S* at a number of stations. It is often easy to detect and pick the first *P* onset times manually since the human eye can identify a change in amplitude or frequency in a signal even in the presence of high noise levels. The picking of *S*-phase onsets is more difficult because these onsets are often emergent and buried in the *P* coda, though at very short ranges the *S* onset can be impulsive and of high amplitude relative to the *P* coda. Automatic detection and picking of phase onsets is much faster and can be more consistent than manual processing; thus, automated methods are necessary for large datasets and for real-time systems. However, robust, automatic, real-time detection and picking of phase onsets on noisy, broadband signals is a difficult algorithmic task.

Real-time seismic monitoring and earthquake early-warning systems must be capable of producing estimates and uncertainties on the location and size of an earthquake beginning a few seconds after the event is first detected (*e.g.*, Kanamori 2005; Zollo *et al.* 2006; Satriano *et al.* 2008). To support this requirement, an automatic phase detector and picker must identify phases and produce robust onset timing, timing uncertainty, onset polarity, and amplitude information, all within the order of 1 second or less of the phase onset time. In addition, for efficiency and because it may be operating within the sensor hardware, a detector and picker must use minimal computing resources, should not require knowledge of detections at other stations, and should not trigger excessively during large events. The picker must operate stably on continuous, broadband signal as output by a sensor digitizer; this signal will in general be noisy and may contain spikes and gaps.

Automatic Detection and Picking Algorithms

Automatic detection and picking algorithms are based on the identification of changes in energy, frequency content, polarization, or other characteristics of the signal relative to the background or long-term level of the corresponding characteristic. Often these algorithms are applied to prefiltered time-series to reduce noise or augment signal in preset or dynamically determined frequency bands or polarization directions. See Withers *et al.* (1998) for a comparison of several approaches.

The most basic and widely used class of methods for phase onset detection and picking is based on comparison between the short-term averages (STA) of a characteristic function (CF) of the signal and a long-term average (LTA) of this CF. These methods are often referred to as STA/LTA or energy methods. In its simplest implementation, the CF might be the absolute value or the square of the signal or its time derivative, and detection declared when the ratio of a short-term average (STA) to a long-term average (LTA) of this function (the STA/LTA ratio) exceeds a predefined or dynamically defined threshold value. After phase onset detection, a pick time and uncertainty may be determined, for example, based on the detection time and the last previous time that the STA/LTA ratio exceeded a lower threshold value, or through additional processing of the signal around the detection time. Two widely used STA/LTA algorithms, the Allen (Allen 1978, 1982) and the Baer-Kradolfer (Baer and Kradolfer 1987; BK87 hereafter) pickers, use CFs based on a combination of the signal and its time derivative at successive samples. The use of the derivative in the CF makes the algorithm more sensitive to changes in the higher frequency content of the signal, as needed for detecting the initial onset times of body-wave phases for local and regional events. The BK87 algorithm uses a combination of the mean and standard deviation of the CF to dynamically set the detection threshold value.

1. ALomax Scientific, Mouans-Sartoux, France
2. Dipartimento di Scienze Fisiche, Università di Napoli Federico II, Naples, Italy; Analisi e Monitoraggio del Rischio Ambientale (AMRA) Scarl, Naples, Italy
3. now at Institut de Physique du Globe de Paris, Paris, France

doi: 10.1785/gssrl.83.3.531

Autoregressive (AR) methods (Sleeman and van Eck 1999; Leonard 2000) are used to determine a pick time after a phase onset has already been detected. AR methods work on the principle that a window of the time-series containing signal from a seismic event has different statistical properties than a window containing noise. Using one or more models for the form of the signal, these methods analyse different subwindows of the time-series to find an optimal point that separates a subwindow with statistical properties of noise from one of noise plus signal. This optimal point determines the pick time.

Other methods for seismic phase detection and picking are based on neural network analysis, polarization analysis, frequency analysis, and other approaches (*e.g.*, Magotra 1987; Cichowicz 1993; Bai and Kennett 2000).

Pickers for Real-Time Seismic Monitoring and Earthquake Early Warning

Many automatic detection and picking algorithms are not suitable for real-time seismic monitoring and earthquake early warning. Some methods, such as AR and those based on polarization and frequency analyses, require a window of signal after initial detection whose length may exceed the required reporting time and thus cannot provide pick information rapidly. Other methods, such as AR, which require a previous pick detection, and those using frequency-domain analyses, introduce computational inefficiencies. In addition, few existing algorithms provide realistic timing uncertainty on the picks, required for developing reliable and informative location uncertainties and probabilistic location information (*e.g.*, Tarantola and Valette 1982; Lomax *et al.* 2000; Lomax 2005; Lomax *et al.* 2009). In general, STA/LTA energy methods provide the best rapidity and computational efficiency needed for real-time and early-warning systems.

Here we introduce a general purpose, broadband phase detector and picker algorithm (FilterPicker) that is applicable to real-time seismic monitoring and earthquake early warning. This algorithm is loosely based on the BK87 and on the Allen picker (Allen 1978, 1982). The FilterPicker algorithm is designed so that it operates stably on continuous, real-time, broadband signals; avoids excessive picking during large events; and produces a realistic time uncertainty on the pick.

THE FilterPicker ALGORITHM

The FilterPicker (FP hereinafter) operates on a discretized time-series signal $y(i)$ with sample interval ΔT. This signal may have little or no preprocessing—it may be a broadband data stream as output from a digitizer without filtering or mean removal. The FP algorithm uses almost exclusively logical and arithmetic operations (*i.e.*, uses the square root, but no exponentials, logarithms, or transform algorithms) and so is computationally highly efficient.

The FP algorithm makes use of decay constants for accumulating time-averaged statistics on the signal independently of the elapsed time since the start of the signal. For a statistic $S = f(y)$, the time-averaged value S_{long} is given by

$$S_{\text{long}}(i) = C_{\text{long}} \cdot S_{\text{long}}(i-1) + \left(1 - C_{\text{long}}\right) \cdot S(i), \quad (1)$$

where $S(i)$ is an instantaneous value of S and $C_{\text{long}}: 0 \le C_{\text{long}} < 1$ is a decay constant defined by $C_{\text{long}} = 1 - \Delta T / T_{\text{long}}$ where T_{long} is a time-averaging scale.

Simple Multiband Processing

To perform broadband picking, we first apply first-differences to the raw broadband signal $y(i)$ to obtain a differential signal, $y'(i)$,

$$y'(i) = y(i) - y(i-1), \quad (2)$$

where $y(0)$ is initialized to the mean of $y(i)$ in the first time interval T_{long}, or the mean of all $y(i)$ if they cover an interval < T_{long}.

Next we generate a set of filtered signals $Y_n(i) = Y_n^{LP}(i)$, $n = 0, N_{\text{band}} - 1$ obtained from $y'(i)$ using two simple one-pole high-pass filters,

$$Y_n^{HP1}(i) = C_n^{HP}\left[Y_n^{HP1}(i-1) + y'(i) - y'(i-1)\right], \quad (3)$$

and

$$Y_n^{HP2}(i) = C_n^{HP}\left[Y_n^{HP2}(i-1) + Y^{HP1}(i) - Y^{HP1}(i-1)\right], \quad (4)$$

followed by one simple one-pole low-pass filter,

$$Y_n^{LP}(i) = Y_n^{LP}(i-1) + C_n^{LP}\left[Y^{HP2}(i) - Y^{HP2}(i-1)\right], \quad (5)$$

with filter constants $C_n^{HP} = w_n/(w_n + \Delta T)$ and $C_n^{LP} = \Delta T/(w_n + \Delta T)$, time constant $w_n = T_n/2\pi$, corner period $T_n = 2^n \Delta T$, and $y'(0)$, $Y_n^{HP1}(0)$ and $Y_n^{HP2}(0)$ initialized to zero. N_{band} is chosen so that $T_{N_{\text{band}}-1} = 2^{N_{\text{band}}-1}\Delta T$ is greater than the largest dominant period of phases to be picked. For example, if $\Delta T = 0.01$ sec and phases with a dominant period of up to 1 sec are to be picked, then N_{band} should be at least ceiling[$\log_2(1/0.01)$] + 1 = 8, giving $T_n(n = 0,7) = \{0.01, 0.02, 0.04, 0.08, 0.16, 0.32, 0.64, 1.28$ sec$\}$. N_{band} should not be set higher than necessary since the overall FP computation time increases directly with N_{band}.

Effectively, Equations 2 through 5 produce simply and efficiently a set of bandpassed time-series with different center periods just under T_n (Figures 1A and 2). The differentiation of Equation 2 serves to augment higher frequencies, while the use of only one one-pole low-pass filter preserves higher frequencies and thus impulsive onsets, relative to the nominal T_n for each band. The resulting time-series for band $n = 0$ is similar to the raw signal twice differentiated; this time series emphasizes the highest frequencies in the signal

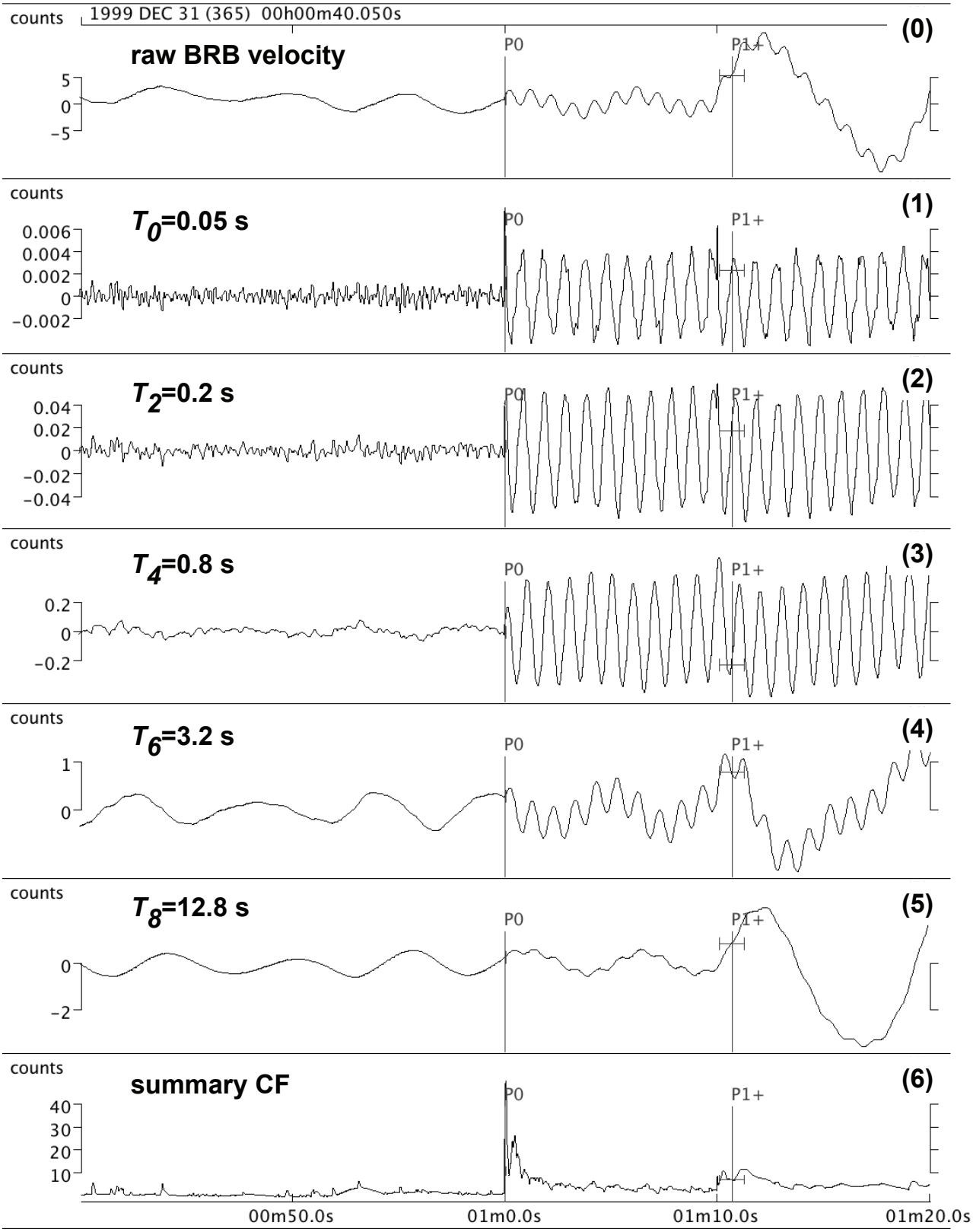

▲ **Figure 1.** Synthetic example of FP multiband filtered traces and picking results. The synthetic time-series is composed of a 1 sec sine signal beginning at 1 m 0.0 sec and a 10 sec sine signal beginning at 1 m 10 sec, superimposed on sine noise around 5 sec plus integrated Gaussian noise. (Data: broadband, 20 samples/sec; Picker (default values): T_{filter} = 15.0 sec, T_{long} = 25.0 sec, S_1 = 10.0 sec, S_2 = 10.0 sec, T_{up} = 1.0 sec). (A) Signals: Trace (0): raw broadband time-series; Traces (1)–(5): filtered signals; Trace (6): summary CF, $F^C(i)$.

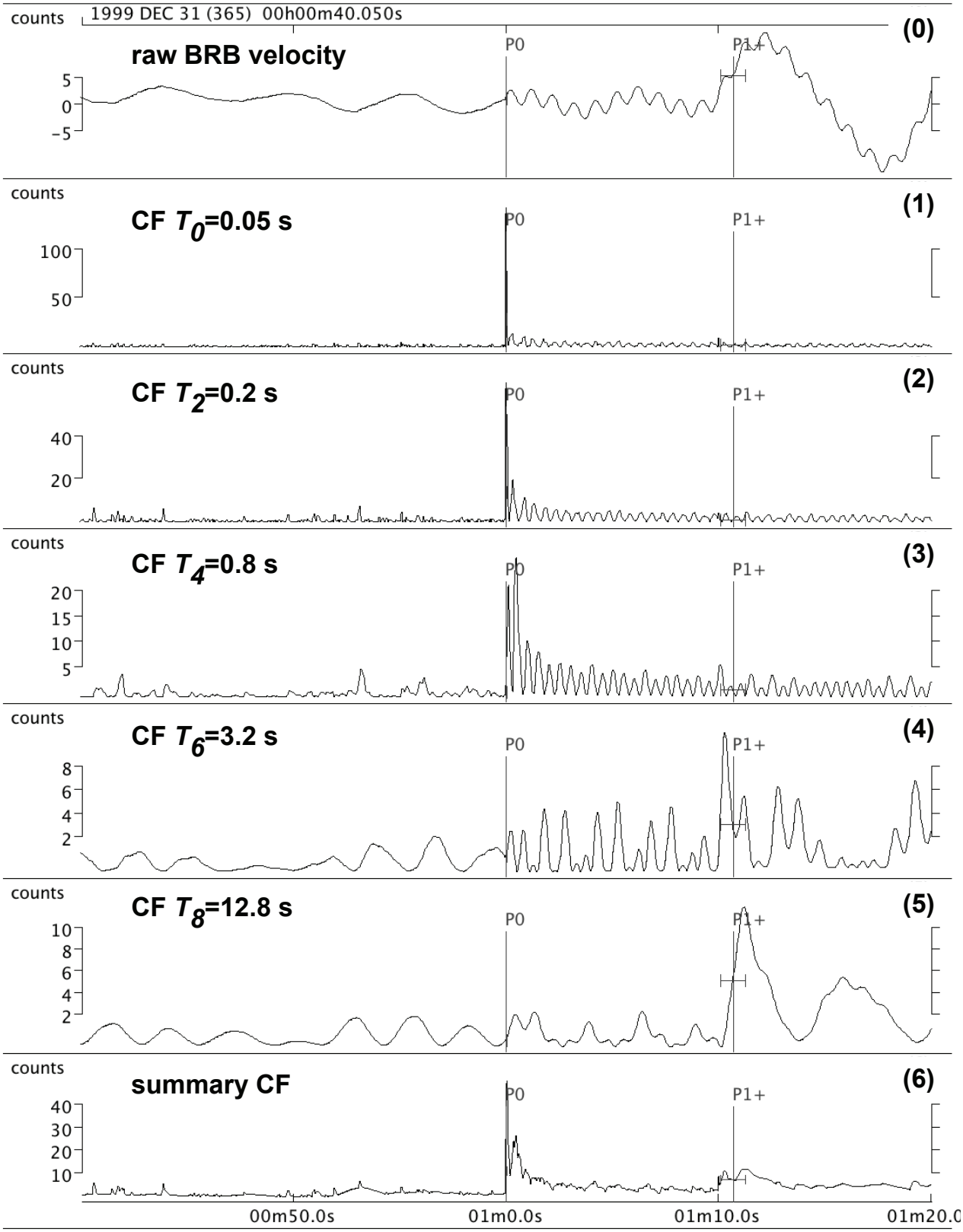

▲ **Figure 1 (continued).** Broadband signal and CFs: Trace (0): raw broadband velocity; Traces (1)–(5): CFs for filtered signals; Trace (6): summary CF, $F^C(i)$. Pick uncertainties shown with a horizontal bar; the uncertainty bar for pick *P*0 is too narrow to appear clearly. The first pick (*P*0) triggered on band $n = 0$ ($T_0 = 0.05$ sec, trace (1)) and the second pick (*P*1) triggered on band $n = 8$ ($T_8 = 12.8$ sec, trace (5)).

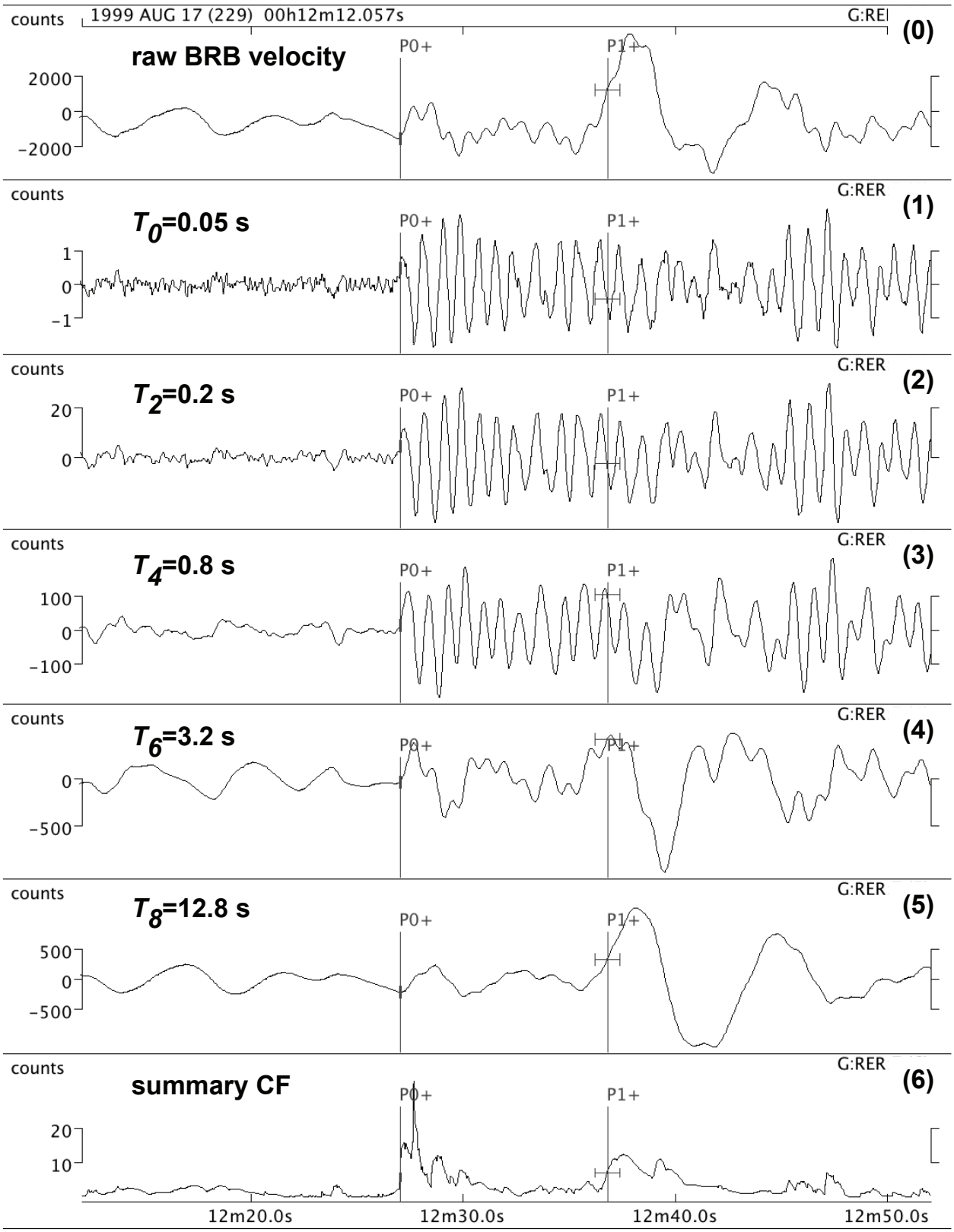

▲ **Figure 2.** Broadband, teleseismic example of FP multiband filtered traces and picking results for 1999.08.17 **M** 7.6 Turkey earthquake recorded at station G:RER. (Data: broadband, 20 samples/sec; Picker (default values): T_{filter} = 15.0 sec, T_{long} = 25.0 sec, S_1 = 10.0 sec, S_2 = 10.0 sec, T_{up} = 1.0 sec). Trace (0): raw broadband velocity; Traces (1)–(5): filtered signals; Trace (6): summary CF, $F^C(i)$. Pick uncertainties shown with a horizontal bar; the uncertainty bar for pick *P*0 is too narrow to appear clearly. The first pick (*P*0) triggered on band $n = 0$ (T_0 = 0.05 sec, trace (1)) and the second pick (*P*1) triggered on band $n = 8$ (T_8 = 12.8 sec, trace (5)).

(*e.g.*, Figures 1A and 2, trace (1)). With increasing n the signal includes longer and longer periods (Figures 1A and 2, traces (1) to (5)).

Characteristic Function

We construct the FP CF, following BK87, by first defining for each band n an envelope function, E_n,

$$E_n(i) = Y_n^2(i), \tag{6}$$

and a characteristic function, $F_n^C(i)$,

$$F_n^C(i) = \frac{E_n(i) - \langle E_n \rangle (i-1)}{\langle \sigma(E_n) \rangle (i-1)}, \tag{7}$$

where $\langle E_n \rangle (i-1)$ and $\langle \sigma(E_n) \rangle (i-1)$, the time-averages up to sample $i-1$ of E_n and the standard-deviation of E_n, respectively, are accumulated using the decay constant C_{long} according to Equation 1. The characteristic function F_n^C (Figure 1B, traces (1) to (5)) quantifies the variation of E_n relative to its background level, represented by the mean value $\langle E_n \rangle$, scaled by $\langle \sigma(E_n) \rangle$, all within the time scale T_{long} corresponding to the decay constant C_{long}.

In a final step, a single, summary CF, $F^C(i)$, is formed by setting $F^C(i) = \max\{F_n^C(i);\ n = 0, N_{\text{band}} - 1\}$ (Figures 1 and 2, trace (6)). The use of the maximum of the CF over all bands to form the summary CF, $F^C(i)$ helps to ensure triggering when a phase-onset has a relatively narrow band-width compared to the background noise, especially when the noise level is similar to or greater than the onset level. An alternate use of, for example, the sum of the CF over all bands as a summary CF would effectively fold noise into the summary CF and make triggering less likely for weaker and narrow-band onsets.

Since the time-average values $\langle E_n \rangle (i-1)$ and $\langle \sigma(E_n) \rangle (i-1)$ vary continuously in response to changes in the background signal levels, $F^C(i)$ is automatically adaptive relative to recent signal levels. In addition, the use of a differential signal (Equation 2) makes $F^C(i)$ insensitive to the absolute signal amplitude (after a stabilization time much larger than the time scale T_{long}), thus the picker can be applied directly to broadband signals that have offsets, microseismic noise, or other noise at periods longer than $T_{N_{\text{band}}}$, *i.e.*, longer than the dominant period of any phases of interest.

Triggering and Pick Declaration

The summary CF $F^C(i)$ (*e.g.*, Figures 1 and 2, trace (6)) is monitored at each time step to check for triggers or pick declarations. A trigger is declared when $F^C(i) \geq S_1$, where S_1 is a predefined trigger threshold, the corresponding trigger time, t_{trig}, is stored, and the highest frequency band (lowest index n) with $F_n^C(i) \geq S_1$ is defined as the trigger band, k. Given a predefined time width, T_{up}, a pick is declared if and when, within a window *up* from t_{trig} to $t_{\text{trig}} + T_{\text{up}}$, the integral of $F^C(i)$, $\Sigma_{\text{up}} F^C(i)\,\Delta T$, exceeds the value $S_2 \cdot T_{\text{up}}$, where S_2 is a predefined threshold. To prevent picking of spikes (a single data point with anomalously large amplitude), the contribution to $\Sigma_{\text{up}} F^C(i)\,\Delta T$ from any data points is limited to $5 \cdot S_1$. Since $F^C(i)$ is the maximum over all bands, the declaration of picks takes into account broadband energy. To avoid excessive picking during larger events, following each declared pick a new pick cannot be declared before $F^C(i)$ drops below $F^C(i) = 2$.

Pick Time, Uncertainty, Polarity, and Strength

Each time the CF, $F_n^C(i)$, for each band n rises past the time-average $\langle F_n^C \rangle$ (accumulated using the decay constant C_{long} according to Equation 1, with $\langle F_n^C \rangle$ constrained to $0.5 \leq \langle F_n^C \rangle \leq S_1/2$), the corresponding sample time is stored as a potential pick time, t_n^{pick}, for the corresponding band. When a pick is declared for trigger band k, if the time difference $t_{\text{trig}} - t_k^{\text{pick}}$ is less than 1/40th the band corner period, *i.e.*, $T_k/40$, then t_{trig} is delayed enough to satisfy this condition. The pick time, t_{pick}, is set to t_k^{pick}. Thus t_{pick} is set near the last point with CF within the pre-phase signal or noise CF for band k, and earlier than t_{trig}, at which there is certainty of phase energy ($F^C(i) \geq S_1$). The pick uncertainty, σ_{pick}, is set equal to the interval from t_{pick} to t_{trig}, giving a pick time with uncertainty specified by $t_{\text{pick}} \pm \sigma_{\text{pick}}$. All figures show examples of the FP setting of the pick time and uncertainty, while Figure 3 shows a detailed view for a first arrival phase. The value $F^C(t_{\text{trig}})$ is taken as an indicator of pick strength.

The polarity of the pick is determined by comparing the sums of the values and the sums of the absolute values of the first differences of the filtered signal values, $Y_k(i)$, between t_k^{pick} and t_{trig}. If the value sum is greater than 66% of the absolute value sum, then the polarity is set as the sign of the value sum; otherwise the polarity is set as unknown. All figures show examples of the FP setting of the pick polarity, while Figure 3 shows a detailed view for a first arrival phase.

VALIDATION AND COMPARISON WITH THE EARTHWORM PICKER

In a companion article (Vassallo *et al.* 2012, this issue) the parameters for the FP (Table 1) and for the picker (PICK_EW) from the Earthworm seismic processing system (Bittenbinder *et al.* 1994) are optimized using a set of local and regional earthquake and noise recordings from the Irpinia Seismic Network (ISNet; Weber *et al.* 2007) in southern Italy. The performance of the optimized FP and optimized PICK_EW are compared using about 6,000 traces of local and regional earthquakes and noise from ISNet; these traces are picked manually and automatically with the two pickers. Relative to PICK_EW, FP produces a higher number of picks corresponding to manual picks (FP 4559, PICK_EW 4271), misses fewer picks that were found manually (FP 489, PICK_EW 777), and produces fewer false picks for which there are no nearby manual picks (FP 537, PICK_EW 644); see Figure 4 in Vassallo *et al.* 2012 (this issue).

In an examination of pick quality as a function of signal-to-noise ratio of the first arrival (Figure 5 in Vassallo *et al.* 2012, this issue), FP, with respect to PICK_EW, is better able to pick

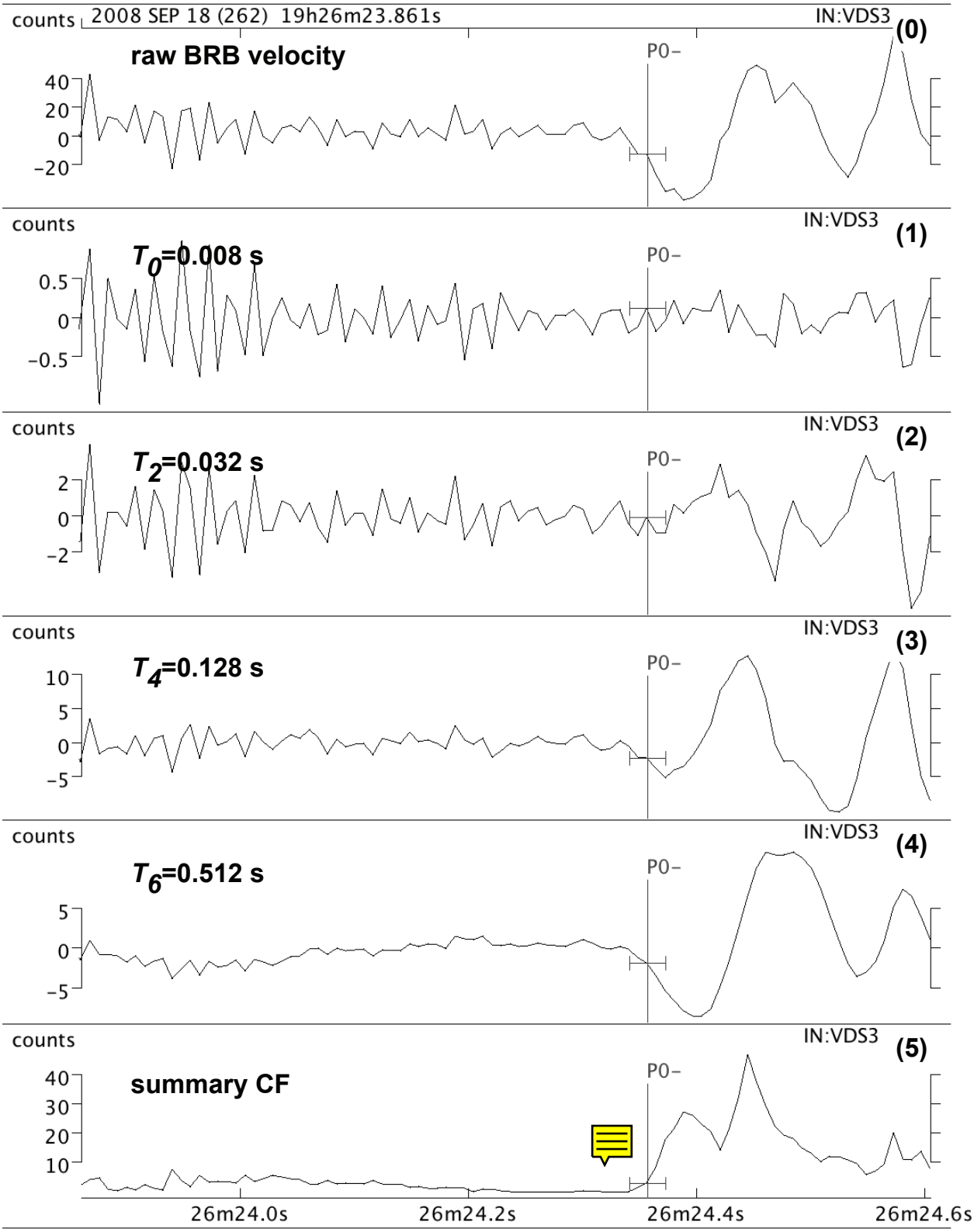

▲ **Figure 3.** Phase onset and pick uncertainty FP example for a small local event recorded at ISNet station VDS3 (Data: broadband, 125 samples/sec; Picker: optimized values from Vassallo *et al.* 2012, this issue, see Table 1). Trace (0): raw broadband velocity; Traces (1)–(4): filtered signals with T_n = 0.008, 0.032, 0.128, 0.512 sec, respectively; Trace (5): summary CF, $F^C(i)$. Pick uncertainty shown with a horizontal bar. The pick (P0) triggered on band n = 5 (T_5 = 0.256 sec, intermediate between traces (3) and (4)). Note the moderate signal-to-noise level; clear, dilatational *P* onset; and pick uncertainty on the raw broadband trace (0). The uncertainty bounds begin before the last sample in the background noise level and end clearly within the onset signal.

the first arrival for all noise levels. For the lowest noise level, class 0, FP misses only 1% of the manual picks compared to 6% missed for PICK_EW. For the highest noise level, class 3, FP misses 22% of the manual picks compared to 29% missed for PICK_EW. Histograms of the differences in time between the automatic and manual picks (Figure 6 in Vassallo *et al.* 2012, this issue) show similar performance for FP and PICK_EW. Both pickers show mean values near 0 sec and small dispersion at lower noise levels, and an indication of delays after the manual picks at the highest noise levels.

The performance of the two pickers is also compared when simulating the complete process of picking, phase association, and event detection within Earthworm. This is done for three different datasets consisting of recordings of 301 events inside the ISNet network, 104 events outside network, and 49 false events recorded primarily during storms (Figure 8 in Vassallo *et al.* 2012, this issue). For events inside the network the total number detected by FP is 282 with 265 detected by PICK_EW. All events with magnitude higher than 2.5 are detected using both pickers, while for the events with magnitude lower than 2.5, the percentage detected by FP is 5–10% higher than by PICK_EW. For events outside the network the total number detected by FP is 76 with 71 detected by PICK_EW. FP detects more events than PICK_EW at most magnitude levels, and FP shows a lower threshold magnitude than PICK_EW for detecting all events. For the false event dataset, processing using FP produces only 10 event declarations, much lower than the 31 events declared using PICK_EW.

APPLICATION EXAMPLES

Application of the FP to a broadband, teleseismic, *P*-wave recording with low signal-to-noise ratio is shown in Figure 2. The picker recovers a higher frequency, impulsive first arrival (*P*0) whose broadband amplitude does not exceed the noise level, and a later, longer-period secondary arrival (*P*1). Figure 3 shows application to a moderate signal-to-noise level but clear, longer-period *P* onset for a local earthquake. The picker picks a dilatation onset on the longer-period multiband traces (traces (3) and (4) in Figure 3), while there is no onset energy visible on the highest frequency trace (1). The picker sets the uncertainty bounds on the pick from approximately the last point clearly in the background noise to the first point clearly in the signal and above the background noise level.

Figure 4 shows application to a low signal-to-noise signal with emergent *P* onset from a small local earthquake. The picker find a first pick (*P*0) where there a clear, impulsive energy on the longer period multiband traces (traces (3) and (4) in Figure 4), though this energy is low amplitude and emergent in the broadband trace (0) and might not be identified by manual picking. A second pick (*P*1) is visible but emergent on the broadband trace (0) but is impulsive on the intermediate bands (traces (3), (4) and (5) in Figure 4). This example indicates how improved triggering and picking for narrower-band phase-onsets and noisy traces follows from the use of the maximum of the CF over all bands to form the summary CF, $F^C(i)$.

The FP picker is currently implemented within the ISNet prototype regional earthquake early-warning system in southern Italy (Satriano *et al.* 2010) and within Early-est, a prototype real-time earthquake location and tsunami-warning monitor running at Istituto Nazionale di Geofisica e Vulcanologia (INGV), Rome (http://early-est.rm.ingv.it). Lancieri *et al.* (2011) successfully employed the FP to pick continuous records of the *Mw* 7.8 Tocopilla, Chile, earthquake sequence.

The FP phase detector and picker is available in the program SeisGram2K (http://alomax.net/seisgram) under the option "Pick->FilterPicker" and as an Earthworm module. Java and C source code for FP are available at http://alomax.net/FilterPicker or from the authors. The default values for the picker parameters are listed in Table 1.

CONCLUSION

FP is a general purpose, broadband phase detector and picker that is applicable to real-time seismic monitoring and earthquake early warning. FP uses an efficient algorithm that operates stably on continuous, real-time broadband signals; avoids excessive picking during large events; and produces onset timing, realistic timing uncertainty, onset polarity, and amplitude information. The FP picker is currently operating successfully

TABLE 1
FilterPicker Parameters

Parameter	Default	Vassallo *et al.* 2012*†	Notes
Filter Window (T_{filter})	$300\Delta T$	0.865 sec = $108\Delta T$	N_{band} = ceiling[$\log_2(T_{filter} / \Delta T)$]
Long Term Window (T_{long})	$500\Delta T$	12.0 sec = $1500\Delta T$	$C_{long} = 1 - T_{long} / \Delta T$
Threshold 1 (S_1)	10	9.36	
Threshold 2 (S_2)	10	9.21	
tUpEvent (T_{up})	$20\Delta T$	0.388 sec = $49\Delta T$	

* optimized using a set of local and regional earthquake and noise recordings from ISNet
† ΔT = 0.008 sec

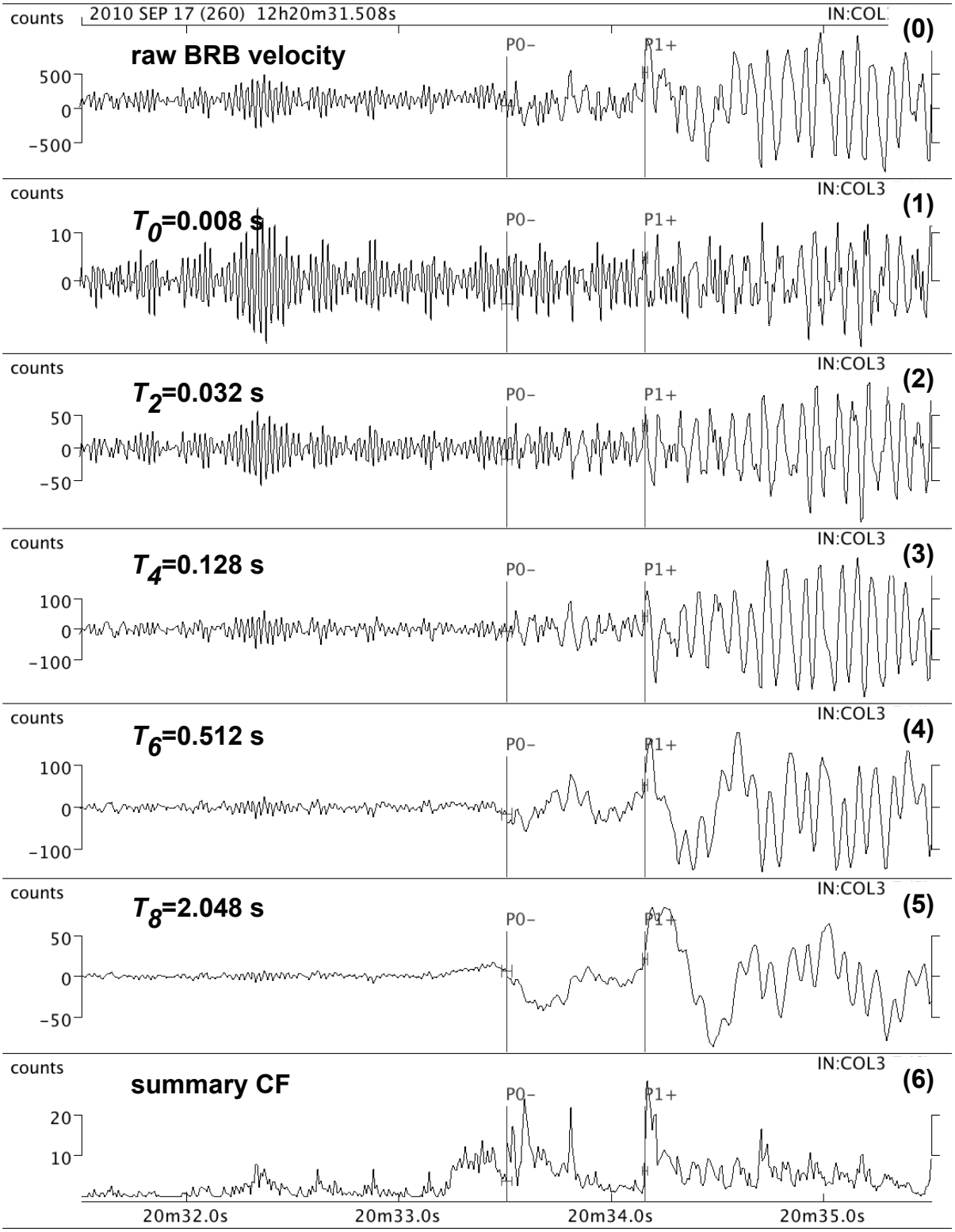

▲ **Figure 4.** Noisy trace example of FP multiband filtered traces and picking results for a small regional event recorded at ISNet station COL3 (Data: broadband, 125 samples/s; Picker (default values): T_{filter} = 2.4 sec, T_{long} = 4.0 sec, S_1 = 10.0 sec, S_2 = 10.0 sec, T_{up} = 0.16 s). Trace (0): raw broadband velocity; Traces (1)–(5): filtered signals; Trace (6): summary CF, $F^C(i)$. Pick uncertainty shown with a horizontal bar. The first pick (P0) triggered on band n = 6 (T_6 = 0.512 sec, trace (4)) and the second pick (P1) triggered on band n = 3 (T_3 = 0.064 sec, intermediate between traces (2) and (3)). Note the low signal-to-noise level and emergent *P* onset on the raw broadband trace (0). The peak in the CF near 20 m 33.3 sec is larger than the trigger threshold, S_1, but does not produce a pick because the condition $\sum_{up} F^C(i) > S_2 \cdot T_{up}$, is not satisfied.

within the ISNet earthquake early-warning system and within the global tsunami-warning monitor at INGV, producing real-time picks and pick uncertainties used for rapid event detection, phase association, event location, and first-motion, fault mechanism determination.

Unlike many pickers, FP has few parameters, all of which are intuitively understandable and not difficult to set. Each FP pick is available at a maximum time of T_{up} after the trigger time or onset of energy; for a 100 samples/sec data stream the default value of T_{up} is 0.2 sec, allowing picking well within the time limits required for determining the location and size of an earthquake for early warning. Investigation and testing of FP within the ISNet and Early-est, and application examples presented here (Figures 1, 2, and 4) show that the default FP parameter settings generally work well. However, Table 1 shows that some of the optimized FP parameters from Vassallo *et al.* 2012 (this issue) differ by up to a factor of 3 from the defaults. These results indicate that, if necessary or convenient, the default picker parameters can be used for many applications, though better picker performance may be obtained through optimization or trial-and error tuning of the parameters.

An optimized FP picker is shown by Vassallo *et al.* 2012 (this issue) to outperform an optimized Earthworm picker, PICK_EW, for detecting and picking local and regional earthquakes at the ISNet in southern Italy. FP, with respect to PICK_EW, gives a greater number of correct picks and fewer false picks. In simulations of the complete process of picking, phase association, and event detection, Vassallo *et al.* 2012 (this issue) find that FP, with respect to PICK_EW, detects more of the true seismic events (in all the magnitude ranges investigated) and produces fewer event declarations for false events.

ACKNOWLEDGMENTS

This research has been funded by Analisi e Monitoraggio del Rischio Ambientale: Analysis and Monitoring of Environmental Risk (AMRA Scarl) through the Seismic Early Warning for Europe (SAFER) project, the EU's Sixth Framework Programme, and through the ReLUIS-DPC project.

REFERENCES

Allen, R. V. (1978). Automatic earthquake recognition and timing from single traces. *Bulletin of the Seismological Society of America* **68**, 1,521–1,532.

Allen, R. V. (1982). Automatic phase pickers: Their present use and future prospects. *Bulletin of the Seismological Society of America* **72**, S225–S242.

Baer, M., and U. Kradolfer (1987). An automatic phase picker for local and teleseismic events. *Bulletin of the Seismological Society of America* **77**, 1,437–1,445.

Bai, C.-Y., and B. L. N. Kennett (2000). Automatic phase-picking and identification by full use of a single three-component broadband seismogram. *Bulletin of the Seismological Society of America* **90**, 187–198.

Bittenbinder, A. (1994). Earthworm: A modular distributed processing approach to seismic network processing. *Eos, Transactions, American Geophysical Union* **75** (44), 430.

Cichowicz, A. (1993). An automatic *S*-phase picker. *Bulletin of the Seismological Society of America* **83**, 180–189.

Kanamori, H. (2005). Real-time seismology and earthquake damage mitigation. *Annual Review of Earth and Planetary Sciences* **33**, 195–214.

Lancieri, M., A. Fuenzalida, S. Ruiz, and R. Madariaga (2011). Magnitude Scaling of Early-Warning Parameters for the *Mw* 7.8 Tocopilla, Chile, Earthquake and Its Aftershocks. *Bulletin of the Seismological Society of America,* **101**(2), 447–463; doi:10.1785/0120100045.

Leonard, M. (2000). Comparison of manual and automatic onset time picking. *Bulletin of the Seismological Society of America* **90**, 1,384–1,390.

Lomax, A. (2005). A reanalysis of the hypocentral location and related observations for the great 1906 California earthquake. *Bulletin of the Seismological Society of America* **95**, 861–877; doi:10.1785/0120040141.

Lomax, A., A. Michelini, and A. Curtis (2009). Earthquake location, direct, global-search methods. In *Encyclopedia of Complexity and Systems Science, Part 5*, ed. R. A. Meyers, 2,449–2,473. New York: Springer; doi:10.1007/978-0-387-30440-3.

Lomax, A., J. Virieux, P. Volant, and C. Berge (2000). Probabilistic earthquake location in 3D and layered models: Introduction of a Metropolis-Gibbs method and comparison with linear locations. In *Advances in Seismic Event Location*, ed. C. H. Thurber and N. Rabinowitz, 101–134. Dordrecht and Boston: Kluwer Academic Publishers.

Magotra, N., N. Ahmed, and E. Chael (1987). Seismic event detection and source location using single station (three-component) data. *Bulletin of the Seismological Society of America* **77**, 958–971.

Satriano, C., L. Elia, C. Martino, M. Lancieri, A. Zollo, and G. Iannaccone (2010). PRESTo, the earthquake early warning system for Southern Italy: Concepts, capabilities and future perspectives. *Soil Dynamics and Earthquake Engineering* **31**, 137–153; doi:10.1016/j.soildyn.2010.06.008.

Satriano, C., A. Lomax, and A. Zollo (2008). Real-time evolutionary earthquake location for seismic early warning. *Bulletin of the Seismological Society of America* **98**, 1,482–1,494; doi:10.1785/0120060159.

Sleeman, R., and T. van Eck (1999). Robust automatic *P*-phase picking: An on-line implementation in the analysis of broadband seismogram recordings. *Physics of the Earth and Planetary Interiors* **113**, 265–275.

Tarantola, A., and B. Valette (1982). Inverse problems = quest for information. *Journal of Geophysics* **50**, 159–170.

Vassallo, M., C. Satriano, and A. Lomax (2012). Automatic Picker Developments and Optimization: A strategy for improving the performances of automatic phase pickers. *Seismological Research Letters* **83**, 541–554. doi: 10.1785/gssrl.83.3.

Weber, E., V. Convertito, G. Iannaccone, A. Zollo, A. Bobbio, L. Cantore, M. Corciulo, M. Di Crosta, L. Elia, C. Martino, A. Romeo, and C. Satriano (2007). An advanced seismic network in the southern Apennines (Italy) for seismicity investigations and experimentation with earthquake early warning. *Seismological Research Letters* **78**, 622–634; doi:10.1785/gssrl.83.3.622.

Withers, M., R. Aster, C. Young, J. Beiriger, M. Harris, S. Moore, and J. Trujillo (1998). A comparison of select trigger algorithms for automated global seismic phase and event detection. *Bulletin of the Seismological Society of America* **88**, 95–106.

Zollo, A., M. Lancieri, and S. Nielsen (2006). Earthquake magnitude estimation from peak amplitudes of very early seismic signals on strong motion records. *Geophysical Research Letters* **33**, L233112; doi:10.1029/ 2006GL027795.

ALomax Scientific
161 Allée du Micocoulier
06370 Mouans-Sartoux France
anthony@alomax.net
(A. L.)